An edited version of this paper was published by AGU. Published 2024 American Geophysical Union.
Kahn, R. A., Limbacher, J. A., Junghenn Noyes, K. T., Flower, V. J. B., Zamora, L. M., & McKee, K. F. (2024). Evolving particles in the 2022 Hunga Tonga—Hunga Ha'apai volcano eruption plume. *Journal of Geophysical Research: Atmospheres*, 129, e2023JD039963. To view the published open abstract, go to https://doi.org/10.1029/2023JD039963

Evolving Particles in the 2022 Hunga Tonga--Hunga Ha'apai Volcano Eruption Plume

Ralph A. Kahn[1,2], James A. Limbacher[3,4], Katherine T. Junghenn Noyes[1,5], Verity J.B. Flower[6], Lauren M. Zamora[1,5], and Kathleen F. McKee[7]

[1]Senior Research Scientist Emeritus, NASA Goddard Space Flight Center, Greenbelt MD 20771.

[2]Now at: The Laboratory for Atmospheric and Space Physics, University of Colorado Boulder, Boulder CO 80303.[3]I. M. Systems Group, Inc. (IMSG), Rockville MD 20850.

[4]National Oceanic and Atmospheric Administration, College Park MD 20740

[5]Earth System Science Interdisciplinary Center, University of Maryland, College Park MD, 20740

[6]University of Stirling, Stirling, FK9 4LA Scotland

[7]Vanderbilt University, Nashville TN 37235.

Corresponding author: Ralph A. Kahn (ralph.kahn@lasp.colorado.edu)

Key Points:

- Even for the optically thin, low-latitude Tonga plume, MISR retrieved aerosol plume-height, associated wind vectors and particle properties
- Parts of near-tropopause and mid-stratosphere aerosol layers were observed downwind over 10 days, nearly all spherical, non-light-absorbing
- The mid-stratosphere particles were smaller, but grew (ANG decreased by >20%) between 1/17 and 1/23, consistent with model predictions

Abstract

The Multi-angle Imaging SpectroRadiometer (MISR) aboard NASA's Terra satellite observed the Hunga Tonga—Hunga Ha'apai (HTHH) 15 January eruption plume on seven occasions between 15 and 23 January 2022. From the MISR multi-angle, multi-spectral imagery we retrieve aerosol plume height geometrically, along with plume-level motion vectors, and derive radiometrically constraints on particle effective size, shape, and light-absorption properties. Parts of two downwind aerosol layers were observed in different places and times, one concentrated in the upper troposphere (11-18 km ASL), and a mid-stratosphere layer ~23 – 30+ km ASL. After the initial day (1/15), the retrievals identified only spherical, non-light-absorbing particles, typical of volcanic sulfate/water particles. The near-tropopause plume particles show constant, medium-small (several tenths of a micron) effective size over four days. The mid-stratosphere particles were consistently smaller, but retrieved effective particle size increased between 1/17 and 1/23, though they might have decreased slightly on 1/22. As a vast amount of water was also injected into the stratosphere by this eruption, models predicted relatively rapid growth of sulfate particles from the modest amounts of SO_2 gas injected by the eruption to high altitudes along with the water (Zhu et al, 2022). MISR observations up to ten days after the eruption are consistent with these model predictions. The possible decrease in stratospheric particle size after initial growth was likely caused by evaporation, as the plume mixed with drier, ambient air. Particles in the lower-elevation plume observed on 1/15 were larger than all the downwind aerosols and contained significant non-spherical (likely ash) particles.

Plain Language Summary

Volcanic eruptions often occur in remote locations, and typically present major hazards for researchers and equipment. This creates opportunities for the frequent, global coverage satellite remote sensing can make from the relative safety of space. Satellite instruments imaged the massive 2022 Hunga Tonga—Hunga Ha'apai eruption plume, mapped the height of the initial injections and distributions of water vapor, SO_2, and aerosol particles. The Multi-angle Imaging SpectroRadiomenter (MISR) instrument aboard NASA's Terra satellite offers some unique capabilities in this respect, by observing the evolving particle properties in two aerosol layers, one near-tropopause and one mid-stratosphere. For about a week following the initial observations on 1/15, the only spherical, non-light-absorbing particles were retrieved by MISR. The particles in the near-tropopause layer had relatively constant, several tenths of a micron effective size. In the mid-stratosphere layer, the particles were systematically smaller, but appeared to grow downwind. As a great deal of water vapor was also injected into the mid-stratosphere, models predicted relatively rapid growth of sulfate particles from modest amounts of SO_2 injected to high altitudes along with the water. The MISR results provide observational support for these model predictions and some constraint on the associated rates, illustrating the contribution satellite remote-sensing can make toward characterizing volcanic plume evolution.

1 Introduction

The Hunga Tonga—Hunga Ha'apai (HTHH) submarine volcano in the South Pacific (20.6˚ S latitude; 175.4˚W longitude) began erupting on 19 December 2021 (Matoza et al., 2022); it produced a moderate eruption at ~03:20 UTC on 14 January; a major explosive event began at ~04:14 UTC on 15 January that propelled considerable material well into the stratosphere, with some reaching into the mesosphere (Amores et al., 2022; Carr et al., 2022; Klein 2022; Proud et al., 2022; Smart, 2022; Zuo et al., 2022). Wave perturbations were detected globally from ground stations and satellites, within the ocean, the land surface, and through the atmosphere up to the ionosphere (Matoza et al., 2022; Themens et al., 2022; Wright et al., 2022). Relatively little SO_2 and HCl were observed in the atmosphere compared to other major volcanic eruptions; for example, the 1991 Mt. Pinatubo eruption ejected ~40 times more SO_2 (e.g., Carn et al., 2022; Millan et al. 2022; Witze, 2022). However, HTHH introduced exceptionally large amounts of water vapor into the stratosphere, up to unprecedented elevation (up to ~58 km) and in quantities not previously observed during the satellite era (Millan et al. 2022; Silletto et al., 2022). Further, significantly more sulfate particles formed and propagated in the stratosphere than would be expected from the relatively modest SO_2 injection of this eruption (Legras et al., 2022; Taha et al., 2022).

The Multi-angle Imaging SpectroRadiometer (MISR) instrument aboard the NASA Earth Observing System's Terra satellite observed parts of the elevated aerosol plume on at least seven occasions between 15 and 23 January, under fair-to-good aerosol-retrieval conditions, as the plume traveled westward, traversing the Coral Sea, Australia, and the Indian Ocean (Figure 1). The MISR retrievals also provide some indication of interaction between the volcanic water and aerosol in the stratosphere as the plume evolved.

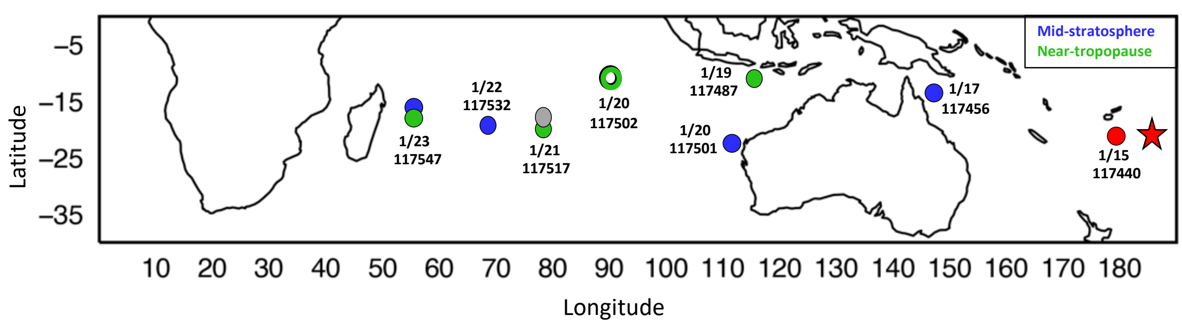

Figure 1. MISR Hunga Tonga—Hunga Ha'apai Volcano-plume-observation *Locations*, *Dates*, and Terra satellite *Orbit numbers*; the volcano is indicated with a red star. Observations of the mid-stratosphere layer, at ~23-30+ km, are shown in blue markers, those of the near-tropopause layer, at ~11-18 km, are shown in green. The red dot indicates where non-spherical particles were retrieved at 10-14 km within a day of the main eruption, most likely dominated by volcanic ash, and the gray dot shows where light-absorbing particles were retrieved, probably smoke originating from wildfires in Australia that might have mixed with the volcanic plume. All other retrievals reported spherical, non-light-absorbing particles, typical of volcanic sulfate/water particles. The open circle marks a downwind plume for which MISR plume heights were retrieved, but the AOD was too low for particle property retrievals.

The Terra satellite's near-polar orbit crosses the equator at approximately 10:30 AM local time. Each of the nine MISR cameras sweeps out a strip of imagery along the spacecraft track on the day side of Earth, successively at angles ranging from 70˚ in the forward direction, through nadir, to 70˚ toward the aft of the spacecraft, in each of four spectral bands centered at 446, 558, 672, and 866 nm (Diner et al., 1998). It takes about seven minutes for all nine cameras to view a given location on Earth. The MISR swath is relatively narrow (~380 km), so sampling is sporadic, especially at low latitudes where the HTHH eruption occurred. Under good, but not necessarily ideal, retrieval conditions, qualitative particle microphysical properties can be derived: three-to-five bins in retrieved, column-effective particle size (REPS), represented in the retrieval results as the Ångström exponent (ANG) or qualitatively as “small,” “medium,” and “large” particles between ~0.1 and ~2 microns effective radius. The exact boundaries of these size bins depend on solar and viewing geometry, AOD, and particle properties, but differences in REPS are much more robust, especially where the observing geometry is quite constant, as for the cases in the current study (Kahn et al., 2001, Kahn and Gaitley, 2015). Under good retrieval conditions, we can also retrieve two-to-four bins in column-effective particle light-absorption (REPA), represented in the retrieval results as the single-scattering albedo at 558 nm wavelength (SSA_{558}), along with spherical vs. randomly oriented non-spherical particles. For the current study, we used the MISR Research Aerosol retrieval algorithm (RA), which offers 1.1 km pixel resolution, the ability to co-register multi-angle views at plume elevation, advanced radiometric calibration, and other refinements aimed at obtaining as much particle property information as possible from the MISR radiances (Limbacher and Kahn, 2014; Limbacher et al., 2022). Due to the stability of the instrument and the satellite, relative differences in REPS and REPA are much more robust than the quantitative ANG and SSA values presented. Our conclusions in this study rely primarily on relative differences in these quantities.

From a volcanological perspective, the particles below a few microns in size to which MISR particle-property retrievals are sensitive represent the lower end of ash components typically emitted during eruptions. However, the MISR-retrieved aerosol optical depth (AOD) captures the extinction of all particles in the column, and the very fine ash and other aerosols within the MISR size-retrieval-sensitivity range probably capture the tail of the full ash size distribution. In themselves, these smaller components have the potential to produce far-reaching effects, as they are the ones more likely to remain suspended in the atmosphere and be transported long distances, impacting the radiative energy balance, air quality and health downwind, as has been observed for other eruptions (e.g., Longo et al., 2010: Sahay et al., 2023; Kluser et al., 2013).

MISR coverage is complemented by imagery from the broader-swath, single-view MODerate resolution Imaging Spectroradiometer (MODIS) instrument, also aboard the Terra satellite, and by layer-height curtains from space-based Cloud-Aerosol Lidar and Infrared Pathfinder Satellite Observation (CALIPSO) lidar, where available. Where plume optical depth is sufficient, 3-D aerosol plume-height maps can be derived geometrically from MISR multi-angle imagery using the MISR INteractive eXplorer (MINX) software tool, with horizontal resolution of 1.1 km and uncertainty in the vertical between 250 and 500 m (Nelson et al., 2013). The MISR stereo-height retrievals have been validated against contemporaneous radar and lidar observations (e.g., Naud et al., 2005; Marchand et al., 2007). MINX is currently configured to retrieve plume altitude values from sea level to an elevation of 30 km. The plume-height retrievals are keyed to the layer of maximum spatial contrast in the atmospheric column; this generally identifies the optically thickest aerosol plume when multiple layers are present, unless meteorological cloud or optically thick aerosol overlies other layers. As such, CALIPSO lidar tends to identify thinner aerosols when they are present at higher elevations, whereas thermal height-retrieval techniques tend to sample systematically lower than MISR/MINX (e.g., Flower & Kahn, 2017). Aerosol plumes are rarely uniform, and MINX retrievals typically obtain a range of elevations for a given plume; although the results are unlikely to capture the absolute top or bottom of an aerosol layer, they often provide an indication of the plume vertical extent. The associated wind vectors at plume elevation are also retrieved from MISR, based on the actual movement of contrast elements in the aerosol plume itself over the seven minutes it takes for all nine MISR cameras to image a given location. These wind vectors also allow for the observed parallax to be corrected for plume proper motion, to produce “wind corrected” stereo heights.

The constraints on particle size, shape, and light-absorption that can be derived from MISR data depend upon the AOD and on the observed range of scattering angles (i.e., the angle from the sun, down into the atmosphere and back up to the cameras). AOD at 558 nm (AOD_{558}) of at least 0.15 or 0.2, but also depending on surface brightness and variability, is required for high-quality particle property retrievals (Kahn and Gaitley, 2015; Limbacher et al., 2022). The HTHH plume data were acquired at nearly the solar equator (~20˚ S latitude in January). This means the range of scattering angles observed by MISR was about the smallest possible, which limits the sensitivity of MISR to particle properties. Nevertheless, the available MISR data do yield some constraints on particle properties and their evolution during the early days of plume transport, as we present here.

In this paper, we summarize the MISR results, as a contribution to the overall picture of this unique event. The instrument observed parts of the HTHH plumes with sufficient AOD to obtain good retrieval results, in relatively cloud-free or broken cloud over-water areas, at least seven times during the 10 days following the initial eruption. A near-source plume segment was captured at an elevation of about 12 km ASL on 15 January (Figure 1, red dot), approximately 18 hours after the largest eruption began. On subsequent days, MISR observed parts of elevated plumes toward the west, near the tropopause at ~11 – 18 km on 19, 21, and 23 January (Figure 1, green dots), and well into the stratosphere at ~23 – 30+ km on 17, 20, 22, and 23 January (Figure 1, blue dots). For 20 January, the open green dot in Figure 1 shows the location of a plume segment for which the plume height was retrieved, but the AOD was too low to derive particle properties. On 21 January, in addition to the near-tropopause south plume segment, an area of light-absorbing particles was retrieved (grey dot in Figure 1), most likely smoke from fires in northern Australia. Both upper and lower layers were observed in the same region on 23 January. In Section 2, we review the MISR plume height, wind vector, and particle property retrieval results. We also use data from the CALIPSO space-based lidar (Winker et al., 2010) and from several AERONET surface stations (Holben et al., 1998), each acquired in the general vicinity of the MISR-observed plumes, to help assess the MISR plume height and particle property results, respectively. In Section 3, we discuss the patterns and present some inferences about plume evolution that we draw from the observations. Brief conclusions are given in Section 4.

2 MISR Observations of the 2022 HTHH Eruption Plume

In this section, we summarize each MISR observation of the HTHH plume between 15 and 23 January 2022, providing our interpretation of the MINX and RA results, including comparisons with the closest AERONET and CALIOP data, where available. We focus on ANG rather than the individual retrieved components, as qualitative differences in ANG are more robust than the components and proportions that the algorithm identifies as providing a match to the observed top-of-atmosphere reflectances. The candidate particle optical models used for the RA retrievals presented here are given in Table S1 in Supplemental Material.

We took several additional steps to maximize confidence in the REPS and REPA results. The cost function used to determine acceptable RA retrieval results is given as:

$$\mathrm{Cost} = \frac{\sum_\lambda \sum_c \left(\frac{\sqrt{w_{\lambda,c}} * \left[BRF_{\lambda,c}^{\mathrm{TOA}} - \mathrm{BRF}_{\lambda,c}^{\mathrm{mod}} \right]}{\mathrm{Unc}_{\lambda,c}} \right)^2}{\sum_\lambda \sum_c w_{\lambda,c}} \quad (1)$$

where $\mathrm{BRF}^{\mathrm{TOA}}$ are the MISR-observed bi-directional reflectance factors as a function of wavelength (λ) and camera (c), $\mathrm{BRF}^{\mathrm{mod}}$ are the model-simulated bi-directional reflectance factors for a given aerosol mixture, and wavelength-dependent optical depth, surface albedo, and atmospheric backscatter fraction, Unc are estimated, channel-specific radiance uncertainties, and *w* are channel-specific weights that account for topographic shadowing, any glint contamination over water, and missing data (details are given in Limbacher & Kahn, 2019 and Limbacher et al., 2022). We examined the dependence of ANG and SSA results on the value of the cost function; for cost function thresholds of 2 and 1 the results are similar in all cases, and the higher threshold provides greater coverage. So, we applied a cost function upper bound of 2 to all the results presented in this paper except for the optically very thick, near-volcano 15 January case.

At low AOD, retrieval sensitivity to particle properties diminishes (e.g., Kahn and Gaitley, 2015). To investigate the relationship between AOD and retrieved particle properties, we plotted the dependence of ANG and SSA on the retrieved AOD. These plots are included as Figures S1 and S2 in the Supplemental Material for the near-tropopause and mid-stratosphere cases, respectively. Retrieved SSA is essentially independent of AOD in all cases after 15 January, whereas ANG tends to increase with increasing AOD_{558}. The ANG variation appears to be real, associated with geographical variation in plume properties shown in subsequent figures. We set a lower bound of 0.15 on AOD_{558} for reporting ANG and SSA statistics to exclude areas where retrieval uncertainty is highest (though this affects only the 21 January case), and an upper bound of 8.0 to help reduce cloud contamination.

Applying these criteria, we examine the seven MISR observations of the HTHH plume:

Table 1. Overview of MISR HTHH Plume Observations

Observation date*	Observation time [UTC]	Approx. Distance from Source [km]	Retrieved Height [km ASL]	Retrieved Zonal winds† [m/s]	Median AOD_{558}	Median ANG
15-Jan	~22:05	340	10 to 14	-10	~3	<~0.4
17-Jan	~00:25	2700	27 to 30+	28	~0.7	~1.4
19-Jan	~2:30	6500	11 to 16	24	~1.1	~0.86
20-Jan	~2:38	7400	24 to 29	32	~0.5	~1.2

21-Jan	~5:00	10750	23 to 26	24	~0.5	~0.94
22-Jan	~5:43	11800	23 to 26	25	~0.4	~1.3
23-Jan	~6:26	12800	15 to 17	12	~0.4	~1.0

*19-Jan main retrieval region; 20-Jan Orbit 117501; 21-Jan South Plume

†Zonal winds are approximate westward median values

15 January 2022, ~22:05 UTC. MISR first imaged the HTHH plume at this time, capturing a swath centered approximately 340 km west of the volcano itself. Figure 2 shows the MISR-retrieved height for this plume segment at 10–14 km ASL. Careful cloud-screening in the MISR RA limits the number of particle property retrievals in the MISR region over which MINX plume heights shown in Figure 2 were derived. High-quality RA retrievals were obtained only on the west side of the study region shown in Figure 3 for this day. AOD_{558} is ~3, the column-effective ANG is <~0.4, indicating a significant contribution from medium-large particles (i.e., >~ a micron in radius), the non-spherical AOD fraction is ~0.16, and the SSA_{558} is ~0.99, all suggesting the presence of some larger, non-spherical volcanic ash or ice particles (see also Table S1). Depolarization and color-ratio observations from CALIPSO also suggest the occurrence of non-spherical ash or ice at elevations up to 40 km on this day (Sellitto et al., 2022). A comprehensive analysis of the 15 January 2022 plume dispersion during the first ~18 hours, includingthese MISR observations and measurements from other sources, is part of continuing work.

On all subsequent days, discussed below, MISR retrieved only spherical, non-light-absorbing particles in downwind plume segments, at elevations from near the tropopause up to the MINX elevation retrieval limit of 30 km ASL.

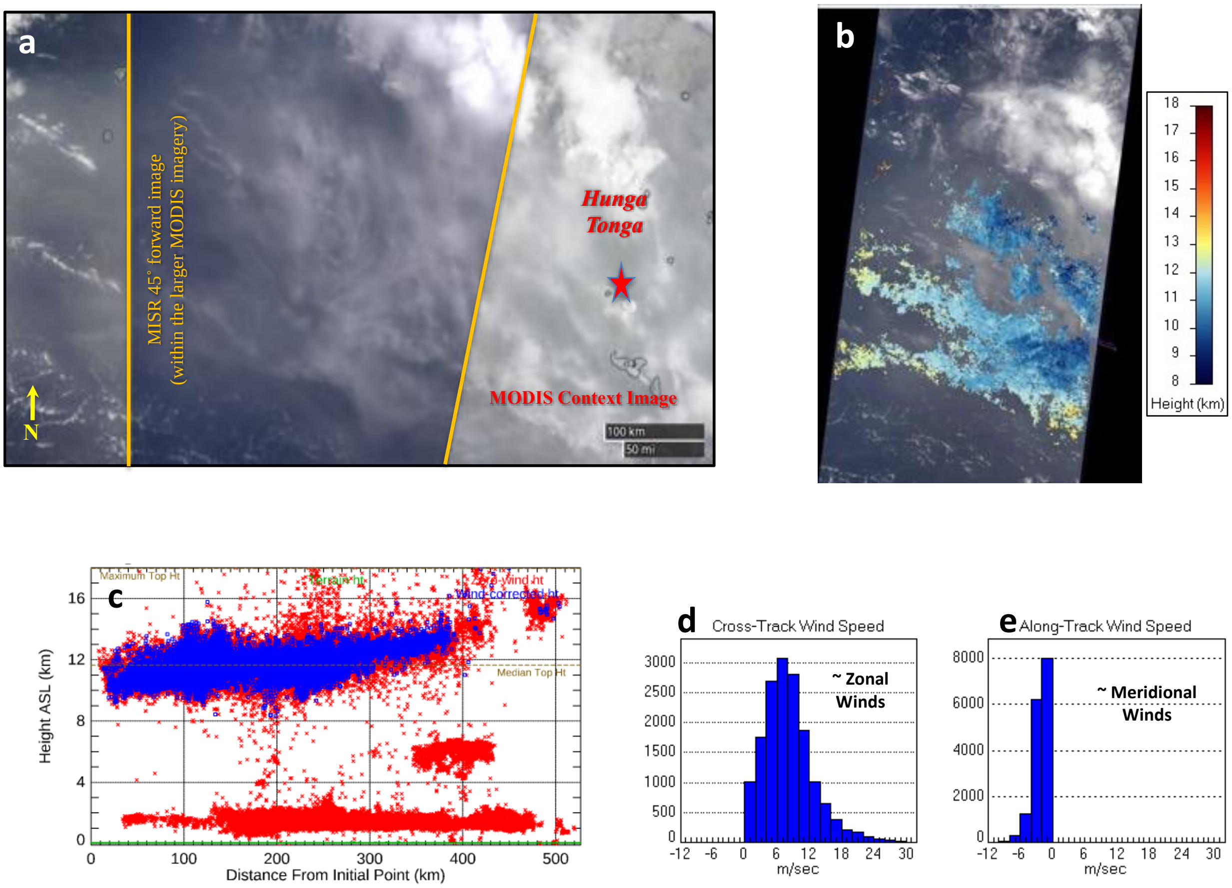

Figure 2. MISR MINX Plume-height and Wind Vector retrieval results for 15 January 2022 at ~22:05 UTC, Terra Orbit 117440. (a) MODIS context image, with MISR 45˚ forward view superposed (between the orange lines). The volcano location is indicated by a red star. (b) MISR MINX plume-height map, superposed on MISR nadir-view image. (c) MISR-retrieved plume-height profile, starting point on the east side of the MISR field-of-view. (d) Cross-track (roughly west-east) and (e) along-track (roughly south-north) MISR-retrieved wind vector components, assessed over all plume points in the digitized region. (Although this plume segment was observed by MISR to the west of the volcano, the retrieved positive zonal wind indicates eastward motion. The zonal winds varied in elevation and time on this day, and an eastward component at the location and time of the MISR observation is supported by National Center for Physical Acoustics reanalysis (NCPA, https://g2s.ncpa.olemiss.edu/). For all other cases in this study, the MISR-retrieved zonal wind is toward the west.) In Panel (c), Red = zero-wind height; Blue = wind-corrected height; Green = surface elevation. No wind-corrected heights were derived for the two lower layers at ~6 km and ~11 km elevation in Panel c, as the origin of digitization was selected for the more prominent layer at ~ 12 km.

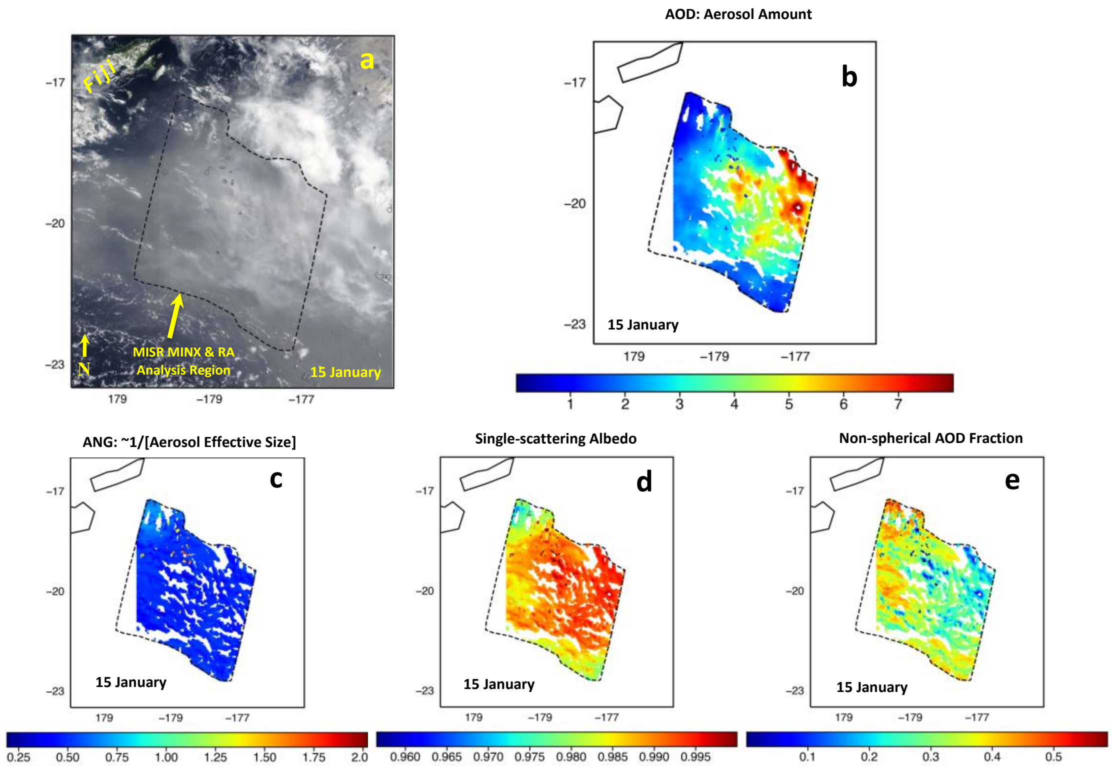

Figure 3. MISR Research Algorithm particle property retrieval results for 15 January 2022, Terra Orbit 117440. (a) MISR context image with study region outlined; the relationship of this region to the HTHH volcano is shown in Figure 2a. (b) AOD_{558} in the less cloudy parts of the study region; (c) ANG assessed between 446 and 866 nm; (d) SSA_{558}; (e) Non-spherical AOD_{558} fraction. No cost-function filter was applied in this one case, but to improve confidence in the particle property retrieval results, ANG and SSA were assessed over the AOD range $0.15 < AOD_{558} < 8.0$. Digital data for the MISR RA results are given in Table S1.

17 January 2022, ~00:25 UTC. On this day, MISR captured a part of the HTHH plume off the northeast coast of Australia, ~2,700 km west of the volcano, and ~450 km north of the Lucinda AERONET site. Plume heights reached from 27 and 30+ km ASL (Figure 4). (As 30 km is the highest elevation allowed by the MINX algorithm, some contrast elements might have occurred above the MINX-reported peak altitude.) AOD_{558} had dropped from the previous MISR plume observation to ~0.7, with ANG ~1.4 (Figure 5 and Table S1). Such small particles provided enough opacity in the MISR blue band (at 446 nm) for contrast features to allow a plume-height retrieval for the 30+ km layer (Figure 4c). However, the elevated plume particles were apparently too small and optically thin in the MISR red band (at 672 nm) to produce sufficient contrast, and only a near-surface layer and a weaker layer around 12 km were retrieved in this channel (Figures 4b). CALIOP lidar confirms the presence of the ~30 km layer in this general area (Figure 4d). The AERONET station at Lucinda obtained contemporaneous measurements of AOD_{550} ~0.7 and ANG ~1.55 (Figures 4f and 4g), confirming to the extent possible the presence of an aerosol layer similar to that retrieved by MISR.

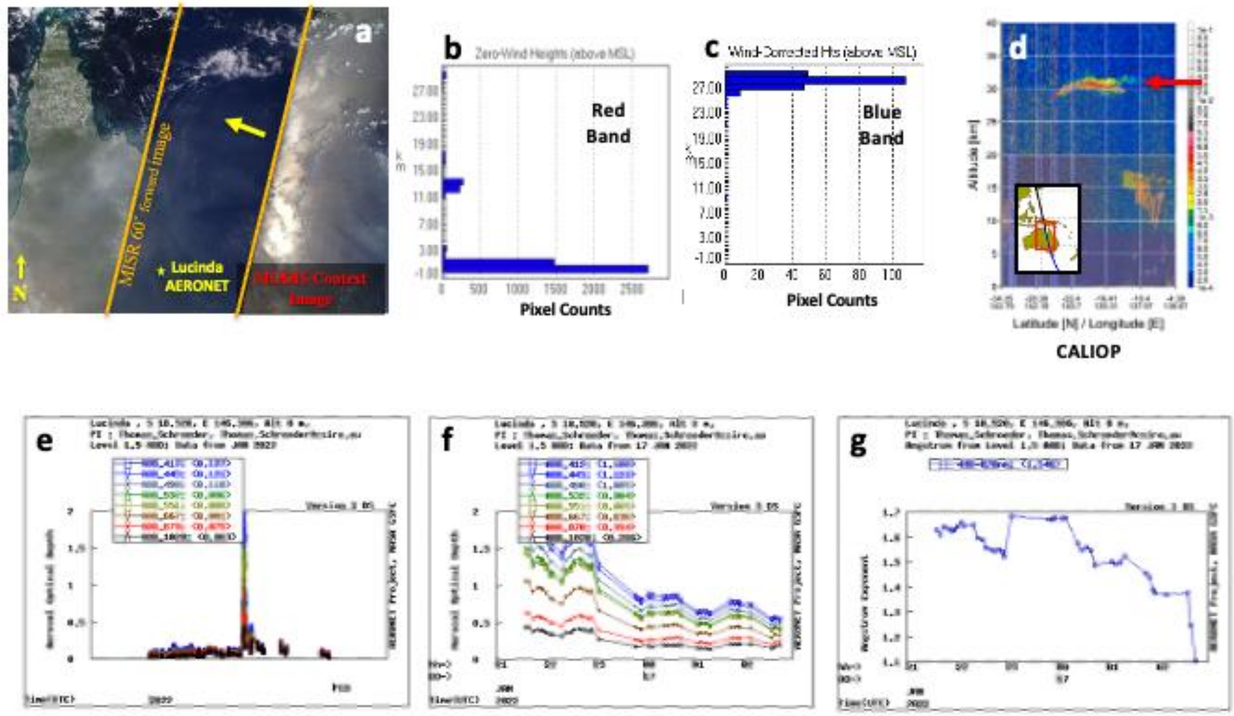

Figure 4. MISR MINX Plume-height retrieval results for 17 January 2022, Terra Orbit 117456, ~00:25 UTC, acquired north of Queensland, Australia, along with Lucinda AERONET ground-station retrievals. (a) MODIS context image, with MISR 60˚ forward view superposed (between the orange lines). The MISR retrieval region is indicated by the yellow arrow. The location of the Lucinda AERONET station on the northeast Australia coast, marked with a yellow asterisk within the MISR swath, ~450 km south of the over-ocean region where the MISR retrievals were performed, was still apparently within the plume. (For scale, the MISR swath is roughly 380 km wide.) (b) Red-band MISR-MINX plume-height histogram, showing a weak layer near the tropopause at 12-14 km and another near-surface. (c) Blue-band MISR plume-height histogram, showing a layer at 27-30+ km. (d) CALIOP Level 1, version 4.51, total attenuated backscatter (km^{-1} sr^{-1}) at 532 nm, acquired at ~05:28 UTC on 17 January, roughly 5 hours after and 800 km downwind of the MISR observation at the nearest point. (The inset gives the orbit location, and the red arrow highlights the likely plume layer.) (e) Lucinda AERONET AOD for 24 January 2022, showing the AOD peak on 17 January. (f) Lucinda AERONET AOD for 17 January 2022. (g) Lucinda AERONET Ångström Exponent for 17 January 2022. (AERONET data were provided by Thomas Schroeder and the AERONET team.)

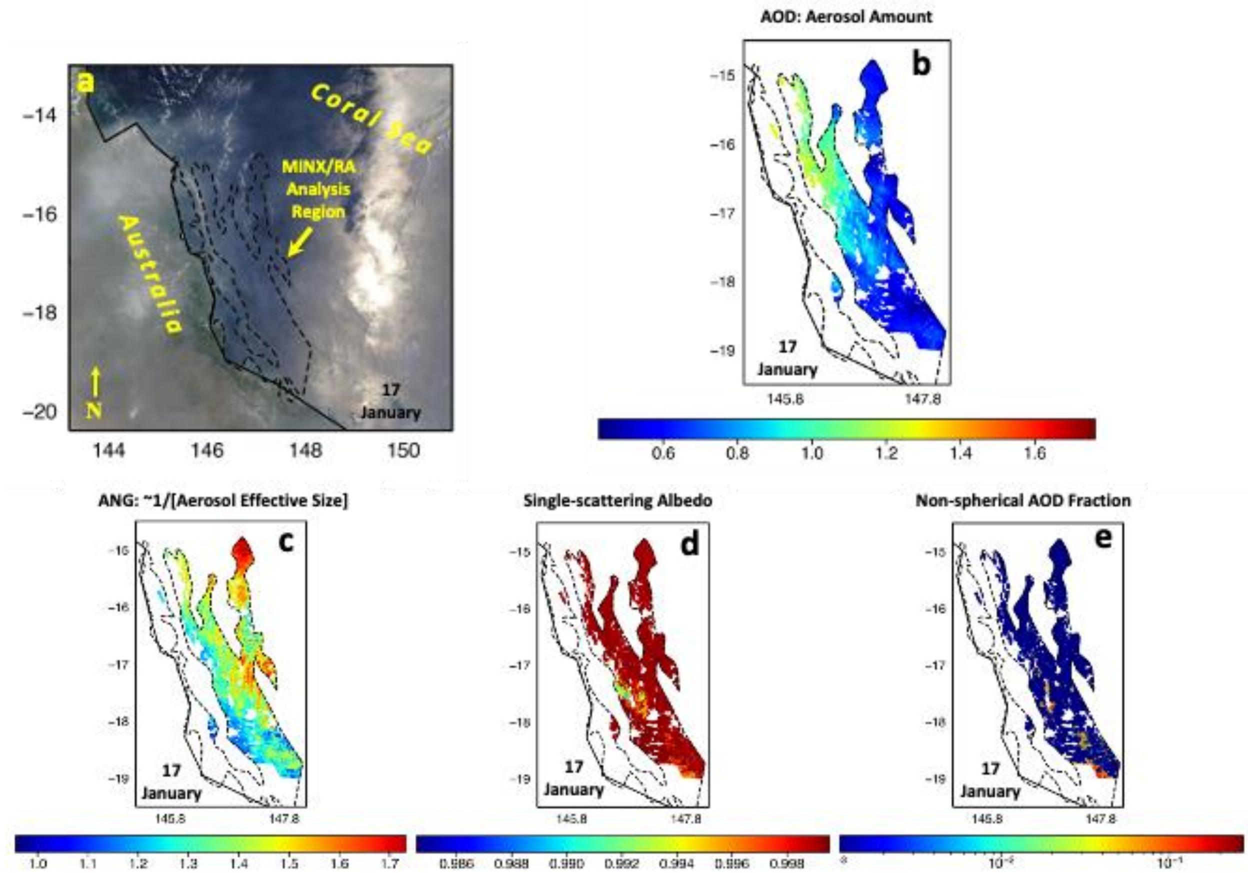

Figure 5. MISR RA particle property retrieval results, same as Figure 3, but for 17 January 2022, Terra Orbit 117456. Note that the scale for panel (e) is logarithmic here to show differences, given the range of in values.

19 January 2022, ~2:30 UTC. MISR observed a plume segment southwest of Java (Figure S3 in Supplemental Material), yielding a plume height of 11-16 km and MINX zonal winds at plume elevation in excess of 24 m/s toward the west. Neither CALIPSO nor ICESat-2 have measurements sufficiently proximal to the MISR observations in space and time to provide validation of the MISR height retrievals. At these low latitudes, the MISR layer would be below, but in the vicinity of, the tropopause elevation. In the least cloud-affected part of the field-of-view, the MISR RA retrieved AOD_{558} ~1.1, ANG ~0.8, with spherical, non-light-absorbing particles dominating (Figure S4 and Table S1).

20 January 2022, ~2:38 UTC. On 20 January MISR observed part of the HTHH plume along the west coast of Australia, about 7,400 km west of the volcano. Here the plume was elevated between 24 and 29 km ASL, with zonal winds of ~30 m/s (Figure S5). CALIOP identified a plume at ~25 – 27 km ASL about 7 hours earlier and 400 km downwind of the MISR observation. MISR median AOD_{558} was about 0.5, most ANG values ~ 1.1, and the particles were again spherical and non-light-absorbing (Figure S6 and Table S1). For comparison, the Learmonth AERONET, about 350 km northeast of the MISR study region along the Australia west coast, obtained AOD_{500} and ANG at the closest observations to MISR overpass time of 0.7 and 1.05, respectively (Figures S6g and S6h). The somewhat larger AOD at the AERONET site could be due to heterogeneity in the aerosol plume after a 5-day transit, with possible contributions from continental aerosol from Australian sources. There was a second MISR overpass of a part of the likely volcanic plume ~2,700 km further west, at ~4:14 UTC. The MISR-MINX retrieval obtained a plume height of 13-17 km ASL, with the hint of another layer at 25-28 km ASL (Figure S7); however, the AOD was too low to derive meaningful particle microphysical properties from the data.

21 January 2022, ~5:00 UTC. The plume observed by MISR on this day was in the central Indian Ocean, about 10,750 km from the source. MISR retrieved a consistent plume elevation of 23-26 km ASL (Figure S8). (ICESat-2 indicated several lower-level aerosol layers between 8 and 12 km, but no retrievals are currently available that sample above 14 km.) The MISR study region on this day contained two plume segments, north and south, that showed distinctly different particle microphysical properties. As with most of the other downwind plume parts captured by MISR, the South segment on 21 January contained small-medium, spherical, non-light absorbing particles, with AOD_{558} ~0.5, ANG ~0.95-1.0, and SSA_{558} ~1.0 (Figure S9 and Table S1).

However, for the North segment, AOD_{558} is ~0.9, ANG is ~1.4-1.5, and SSA_{558} is between 0.94 and 0.96 (Figure S10 and Table S1). The low SSA_{558} and smaller effective particle size suggest the North segment might contain smoke. This seems likely, as major fires were burning in northeast and northwest Australia, producing extensive smoke plumes visible in MODIS imagery from 16 to 18 January (https://worldview.earthdata.nasa.gov; last accessed 01 May 2023). Trajectory analysis from NOAA's HySPLIT model (Rolph et al., 2017) indicates that transport from across north Australia to the location of the MISR plume observation on 21 January (~21.4˚S, 77.3˚E) occurred in 3-4 days at elevations from 18 to over 27 km. This result also represents a demonstration of our ability to derive distinct aerosol type differences from the MISR multi-angle, multi-spectral data.

22 January 2022, ~5:43 UTC. MISR observed a plume segment at 23-26 km ASL on 22 January, about 11,800 km from the source (Figure S11). Yet, the MISR RA derived a mean AOD_{558} around 0.4, within the range for which particle properties can be retrieved over dark water (Figure S12 and Table S1). The particles are all of small size (ANG ~1.3) and are still spherical and non-light absorbing, as for all previous downwind retrievals associated with the volcano plume.

23 January 2022, ~6:26 UTC. This was the final occasion on which MISR captured a segment of the HTHH eruption plume having sufficient definition to report plume elevations with some confidence. In this case, we derive particle microphysical properties qualitatively in two distinct layers. By the time of these observations, the plume particles had reached the vicinity of Réunion Island, ~12,800 km west of the volcano and ~720 km east of Madagascar. The lower layer was concentrated 15-17 km ASL, whereas the thinner upper layer concentrated at ~24-26 km above the ocean surface, extending over the lower layer as well as to the northwest and southeast of the lower layer (Figure S13b, c). The MISR retrieval indicates westward motion at ~ 8-12 m/s (Figure S13e, f). For the "mixed-height" layer, dominated by the lower, optically thicker layer, total-column AOD_{558} was retrieved at ~ 0.4 and ANG ~1.0 (Figure S14 and Table S1). For the elevated layer alone, AOD_{558} was <~ 0.3 and ANG ~1.1. The AERONET site at Réunion, just north of the MISR retrieval region, reported AOD500 ~0.4 and ANG ~0.63 at the 6:26 UTC MISR overpass time, i.e., larger particles than those observed by MISR (Figure S13).

There was also a stratospheric balloon flight deployed from La Réunion island itself (21.1˚ S; 55.3˚ E) on this day (20:04 – 21:35 UTC), carrying an optical counter with sensitivity to particle sizes from 0.2 μm to ~30 mm diameter in 19 bins (Kloss et al., 2022). They also had a ground-based backscatter lidar. The balloon identified plume layers at 22.6 and 24.9 km ASL, the upper layer corresponding to the upper layer identified by MISR (Fig. S13c, d). The lower layer identified by MISR is about 6 km below the lower layer reported by the *in situ* measurements. (There are also discrepancies in layer elevations between the balloon and the ground-based lidar, likely due to differences in spatial sampling combined with layer heterogeneity.) Consistent with the MISR results, the optical counter found spherical, non-light absorbing particles with radii <0.5 μm in the upper layer. In their 22.6 km layer, they report some light-absorbing particles, which could be transported smoke, as we observed with MISR on 21 January.

3 Discussion – MISR Constraints on the Evolution of the HTHH Aerosol Plume

The altitude reached by volcanic emissions depends on ejection force, plume buoyancy, atmospheric stability profile, wind shear, and particle properties. Generally, ash particles are likely to settle more rapidly than smaller, lighter, aerosol components, especially those that tend to form after eruption from water vapor and other gases, such as typical sulfate/water particles in volcanic plumes. On 15 January, MISR retrieved particles containing a significant fraction of non-spherical components, with ANG <~0.4, indicating medium-large particles (Table S1), most likely dominated by volcanic ash. A complimentary study by *Sellitto et al*. (2022) concluded that ash was deposited rapidly between 19:00 UTC on 15 January and 02:00 UTC on 16 January, based on frequent observations made with the geostationary Himawari 8 satellite. The MISR observation, obtained at 22:05 UTC on 15 January, falls within this window. As such, the MISR observation was likely acquired during a period of rapid ash deposition. MISR ash detection on this day is further supported by the lack of ash markers identified in subsequent MISR retrievals; between 17 and 23 January MISR retrievals consistently found spherical, non-light-absorbing aerosols, more likely composed of sulfate/water than ash. (The other exception occurred on 21 January, when in addition to the volcanic plume, MISR observed what was likely transported smoke (Figure S10).) We note that Colombier et al. (2023) posit non-spherical sea salt particles might be part of the 15 January atmospheric aerosol load, given the submarine nature of the eruption and the presence of sea salt in surface samples acquired on nearby islands. With MISR we cannot distinguish such particles from ash, so our data have nothing to contribute about this possibility.

Other satellite observations identified an SO_2 gas plume ejected during the HTHH eruption and tracked the resulting sulfate particles to altitudes exceeding 45 km (*Sellitto et al*., 2022; *Taha et al*., 2022), possibly up to where the plume achieved neutral buoyancy and/or where ambient conditions, such as the anomalously high concentration of water vapor, favored rapid sulfate formation through oxidation and hydration processes. The apparent vertical separation of sulfate/water and ash plumes has also been observed in other volcanic eruptions, such as Grimsvotn in 2011 (*Flower & Kahn*, 2020). Preferential settling of ash likely contributed to the lack of larger, non-spherical particles observed further downwind from the volcano after

15 January. The observation of localized ash-fall around the volcano immediately following the eruption (e.g., *Thompson*, 2022) also supports the rapid-ash-deposition hypothesis.

Two aerosol layers were observed in the downwind MISR plume detections, one near-tropopause and one mid-stratosphere. For the near-tropopause layer, AOD_{558} exceeded unity on 19 January, diminishing to ~0.47 on 21 January (South plume) ~0.4 on 22 January, and 0.26 by 23 January in the MISR retrievals (Table S1). These retrievals indicate spherical, non-light-absorbing particles, with median ANG between 0.85 and about 1.0, i.e., small-medium particles. possibly decreasing very gradually in effective size (Figure 6). With the sparse MISR sampling of these extended aerosol layers, plume heterogeneity is likely, so the values reported should be considered qualitatively representative of overall plume properties during transport, with higher confidence in the relative changes than the absolute values. The North plume segment on 21 January has distinctly different microphysical properties than the adjacent South plume segment observed at the same elevation: significantly higher median AOD_{558} (~0.9), lower SSA_{558} (~0.96), and larger ANG (~1.5). The North plume properties are typical of transported wildfire smoke, and model trajectories from burning regions in parts of north Australia support this suggestion (see Section 2 above). These results also contribute to validating the qualitative MISR particle microphysical property retrievals, as they show distinctions that are at least consistent with the available independent, circumstantial evidence.

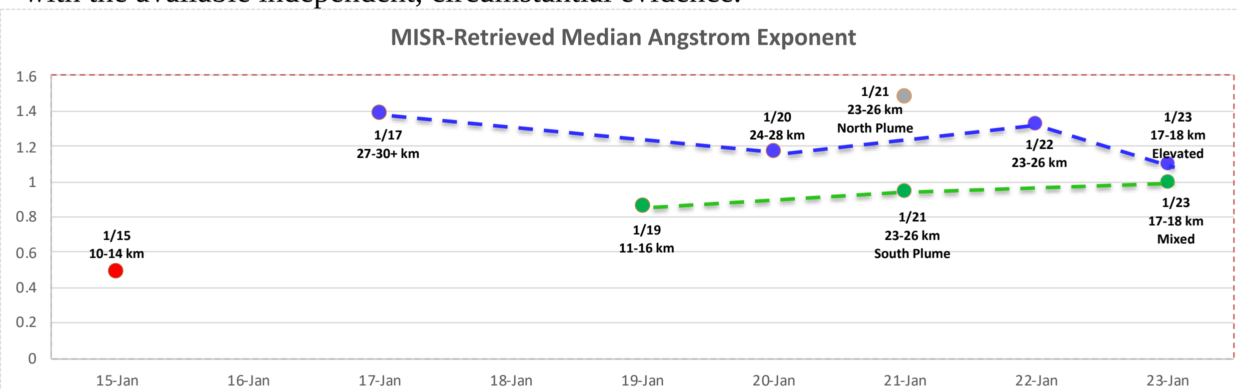

Figure 6. MISR-retrieved Ångström exponent (ANG, inversely proportional to effective particle size) for the MISR observations of the near-source HTHH plume on 15 January (red dot), and for the near-tropopause (green dots) and stratosphere (blue dots and gray dot) plumes downwind. Observation dates and plume heights are given in the annotations.

AOD_{558} in the mid-stratosphere layer diminished systematically from about 0.7 to ~0.26 between 17 and 23 January (Table S1). Essentially spherical, non-light-absorbing particles were retrieved in all cases for this layer. Of particular interest is the effective particle size, which is inversely proportional to the MISR-retrieved ANG plotted for the available cases in Figure 6. For the plume segments in the mid-stratosphere layer (blue dots), the effective particle size was always smaller than that for the near-tropopause layer (green dots), and the retrieved effective particle size (REPS) actually increased between 17 and 20 January, then appears to have decreased by 22 January and possibly increased again in the lowest-AOD observation on 23 January. From the available snapshots, particle evolution can only be inferred; if these observations capture the evolution of particles in the layer near 30 km, either coagulation of particles in the layer or the condensation of water might be responsible for the observed particle growth. The layer mid-visible optical depth was ~0.4 on 22 January (Table S1) and the layer vertical extent was at least 5 km (Figure S11c), so particle concentrations were fairly low, which does not favour particle collision and coagulation. However, an unprecedented amount of water vapor was present at these elevations; ordinarily, the stratosphere at ~30 km is very dry, whereas HTHH was a “wet” eruption, and Microwave Limb Sounder (MLS) data show that significant water was injected to these elevations (*Millan et al*., 2022). This supports an explanation for the apparent particle growth as the result of particle hydration, either by adsorption or by ice deposition. Ice deposition on volcanic particles is a well-known phenomenon in wet (i.e., phreatomagmatic) eruption plumes (e.g., Van Eaton et al., 2012), an example of the classic juxtaposition of fire and ice.

4 Conclusions

As the MISR swath-width is relatively narrow, inferences drawn about HTHH plume evolution from the snapshots of this low-latitude eruption presented here must be considered in the context of broader-swath observation provided by other instruments, as cited above. Yet, MISR does contribute unique information, particularly about changes in height-resolved particle properties during the week following the eruption. The MISR-retrieved spectral AOD results generally align with those obtained by ground-based sun photometers, which provide some validation for the MISR aerosol amount (AOD) and particle size (ANG) retrievals. Similarly, three cases where the CALIPSO lidar observations of plume height were sufficiently close in space and time to the MISR observations support the MISR-MINX plume-height results.

MISR captured two distinct layers of the HTHH eruption plume downwind, one near-tropopause and one mid-stratosphere. On 15 January, a plume rich in medium-large, non-spherical particles (likely volcanic ash) was observed a few hundred kilometers to the west of the volcano. Thereafter, only small or small-medium, spherical, non-light-absorbing particles, typical of volcanic sulfate/water, were retrieved by MISR. By 23 January, the sulfate-like HTHH aerosol plume had remained suspended for more than a week, had travelled at least a third of the way around the globe, and was still sufficiently optically thick to support MISR plume-height and particle-property retrievals, though with somewhat lower confidence than the higher-AOD cases.

Particles in the mid-stratosphere layer (blue dots in Figures 1 and 6) were systematically smaller than the near-tropopause particles (green dots). The mid-stratosphere particles apparently grew in size between 17 and 20 January, likely due to hydration or water condensation, then seem to have fluctuated in size between 22 and 23 January, possibly due to some combination of measurements sampling different parts of a heterogeneous plume and evaporation as the plume mixed with drier air and dissipated downwind. For the near-tropopause layer, particle size remained relatively constant or very gradually diminished between 19 and 23 January. Due to the stability of the instrument and the satellite, these relative size differences, retrieved from MISR, are much more robust than absolute values. As such, our main conclusions rely on relative differences in particle microphysical properties and showconsistency with model predictions (e.g., Zhu et al., 2022).

We note also that after we originally submitted the current paper, several preliminary studies appeared relevant to key aspects of our conclusions. Specifically, Biochu et al. (2024) combined HIMAWARI-8 geostationary thermal infrared imagery with CALIPSO lidar to identify ash on 15 January, and subsequently smaller, but initially rapidly growing, stratospheric aerosol with estimated 0.3-0.5 μm radius, which they interpret as sulfate and track for up to 1.4 years thereafter. They support their satellite-data interpretation with measurements from multiple low-latitude AERONET stations, including the Lucinda and Learmonth stations that we use for validation in the current study. Gupta et al. (2024) used Stratospheric Aerosol and Gas Experiment-III (SAGE-III) observations to characterize stratospheric aerosol amount and extinction associated with the HTHH eruption; they highlight the importance of knowing the sulfate aerosol amount and properties, showing that although water vapor added to the stratosphere would produce surface warming, this would be offset by a net cooling due to stratospheric ozone loss and sulfate aerosol production.

The MISR results presented here demonstrate our space-based multi-angle, multi-spectral aerosol retrieval capabilities, and represent the MISR contribution to ongoing investigations by the wider community aimed at deriving as much as possible about HTHH plume-particle evolution from satellite remote-sensing data and modelling.

Acknowledgments

The authors declare no conflicts of interest. This work is part of the interdisciplinary Volcanology from Space project, supported in part by the NASA Atmospheric Chemistry Modeling and Analysis Program (ACMAP) under Dr. Richard Eckman, the NASA Earth Observing System Terra and MISR projects, and the NASA Earth Surface and Interior program under Benjamin Phillips. We thank our colleagues on the MISR team at the Jet Propulsion Lab and the NASA Langley Atmospheric Sciences Data Center for their roles in producing and archiving the Level 1 MISR data used in this study.

Open Research

MISR data are freely available for download from NASA's MISR data repository (https://l0dup05.larc.nasa.gov/MISR/cgi-bin/MISR/main.cgi), maintained by the NASA Langley Research Center (LaRC) Atmospheric Science Data Center (ASDC). The MISR INteractive eXplorer (MINX) program, for determining plume altitude and associated motion vertors, is a stand-alone software package developed at the NASA Jet Propulsion Laboratory (JPL) and distributed through Github (https://github.com/nasa/MINX/releases). MODIS true color imagery are accessed through the NASA Worldview application (https://worldview.earthdata.nasa.gov), part of the NASA Earth Observing System Data and Information System (EOSDIS). The AERONET and CALIPSO data are freely available from their respective archives at https://aeronet.gsfc.nasa.gov and https://subset.larc.nasa.gov/calipso/. MISR RA and MINX results generated in this work will be accessed through the NASA Langley ASDC, where the MISR Standard Products are also archived (https://eosweb.larc.nasa.gov/project/MISR). All the results of the study are presented in the paper itself and supplemental material, including the key data statistics associated with this study.

References

Amores, A., Monserrat, S., Marcos, M., Argüeso, D., Villalonga, J., Jordà, G., & Gomis, D. (2022). Numerical simulation of atmospheric Lamb waves generated by the 2022 Hunga-Tonga volcanic eruption. *Geophys. Res. Lett., e2022GL098240*, doi:10.1029/2022GL098240.

Boichu, M., R. Grandin, L. Blarel, B. Torres, Y. Derimian, P. Goloub, C. Brogniez, I. Chiapello, O. Dubovik, T. Mathurin, N. Pascal, M. Patou, and J. Riedi (2024). Growth and global persistence of stratospheric sulfate aerosols from the 2022 Hunga Tonga-Hunga Ha´apai volcanic eruption. Preprint from ESS Open Archive, 16 January, 2024. Doi: 10.22541/essoar.168565384.43597078/v2.

Carn, S., Andrews, B., Aquila, V., Cauley, C., Colarco, P., Dufek, J., Fischer, T., Kenis, L., Krotkov, N., Li, C., Mastin, L., Newman, P., & Wallace, P. (2022). Satellite observations and modeling of the 2022 Hunga Tonga-Hunga Ha'apai eruption, EGU General Assembly 2022, Vienna, Austria, 23–27 May 2022, EGU22-13583, doi:10.5194/egusphere-egu22-13583.

Carr, J.L., Horváth, Á., Wu, D.L., & Friberg, M.D. (2022). Stereo Plume Height and Motion Retrievals for the Record-Setting Hunga Tonga-Hunga Ha'apai Eruption of 15 January 2022. *Geophys. Res. Lett. 49, e2022GL098131*. doi:10.1029/2022GL09813.

Colombier, M., I.A. Ukstins, S. Tegtmeier, B. Scheu, S.J. Cronin, S. Thivet, J, Paredes-Marino, et al. (2023). Atmosphere injection of sea salts during large explosive submarine volcanic eruptions. *Nat. Sci Rep 13, 14435*. doi:10.1038/s41598-023-41639-8.

Diner, D.J., J.C. Beckert, T.H. Reilly, C.J. Bruegge, J.E. Conel, R.A. Kahn, J.V. Martonchik, T.P. Ackerman, R. Davies, S.A.W. Gerstl, H.R. Gordon, J-P. Muller, R. Myneni, R.J. Sellers, B. Pinty, and M.M. Verstraete, 1998. Multiangle Imaging SpectroRadiometer (MISR) description and experiment overview, *IEEE Trans. Geosci. Remt. Sensing 36, 1072-1087*, doi: 10.1109/36.700992.

Flower, V.J.B., and R.A. Kahn (2017). Assessing the altitude and dispersion of volcanic plumes using MISR multi-angle imaging: Sixteen years of volcanic activity in the Kamchatka Peninsula, Russia. J. Volcanology and Geothermal Research 337, 1–15, doi: /10.1016/j.jvolgeores.2017.03.010.

Flower, V.J.B., & Kahn, R.A. (2020). The evolution of Iceland volcano emissions, as observed from space. *J. Geophys. Res., 125, e2019JD031625*, doi:10.1029/2019JD031625.

Gupta, A., T. Mittal, K. Fauria, R. Bennartz, and J. Kok (2024). The January 2022 Hunga eruption cooled the southern hemisphere in 2022. Preprint from Research Square on 16 January 2024. https://assets.researchsquare.com/files/rs-3493146/v1_covered_da770520-9f87-4542-a6c2-ba916851c72e.pdf.

Holben, B. N., Eck, T. F., Slutsker, I., Tanré, D., Buis, J. P., Setzer, A., et al. (1998). AERONET — A federated instrument network and data archive for aerosol characterization *Remt. Sens. Environ., 66, 1–16*, doi:10.1016/S0034-4257(98)00031-5.

Kahn, R.A**.**, P. Banerjee, and D. McDonald (2001). The Sensitivity of Multiangle Imaging to Natural Mixtures of Aerosols Over Ocean, *J. Geophys. Res.106*, 18219-18238, doi: 10.1029/2000JD900497.

Kahn, R.A., & Gaitley, B. J. (2015). An analysis of global aerosol type as retrieved by MISR. *J. Geophys. Res. Atmos. 120, 4248-4281*, doi:10.1002/2015JD023322.

Klein, A. (2022). Tongan volcano erupts. *New Scientist, 253(3370) 7*, doi:10.1016/s0262-4079(22)00074-4.

Kloss, C., Sellitto, P., Renard, J.-B., Baron, A., Bègue, N., Legras, B., et al. (2022). Aerosol characterization of the stratospheric plume from the volcanic eruption at Hunga Tonga 15 January 2022. *Geophys. Res. Lett. 49, e2022GL099394*. doi:10.1029/2022GL099394

Kluser, L., T. Erbertseder, and J. Meyer-Arnek, 2013. Observation of volcanic ash from Puyehue–Cord´on Caulle with IASI. *Atmos. Meas. Tech., 6, 35–46, 2013*. doi: 10.5194/amt-6-35-2013.

Legras, B., C. Duchamp, P. Sellitto, A. Podglajen, E. Carboni, R. Siddans, J-U. Groos, S. Khaykin, and F. Ploeger (2022). The evolution and dynamics of the Hunga Tonga–Hunga Ha'apai sulfate aerosol plume in the stratosphere. *Atmos. Chem. Phys., 22, 14957–14*970, doi: 10.5194/acp-22-14957-2022.

Limbacher, J.A., & Kahn, R.A. (2014). MISR Research-Aerosol-Algorithm: Refinements For Dark Water Retrievals. *Atm. Meas. Tech. 7, 1-19,* doi:10.5194/amt-7-1-2014.

Limbacher, J.A., Kahn, R.A., & Lee, J. (2022). The New MISR Research Aerosol Retrieval Algorithm: A Multi-Angle, Multi-Spectral, Bounded-Variable Least Squares Retrieval of Aerosol and Surface Properties. *Atmosph. Meas. Tech. 15, 6865–6887*, doi:10.5194/amt-15-6865-2022.

Longo, B. M., Yang, W., Green, J. B., Crosby, F. L., & Crosby, V. L. (2010). Acute health effects associated with exposure to volcanic air pollution (vog) from increased activity at Kilauea Volcano in 2008. *Journal of Toxicology and Environmental Health, Part A, 73(20),* 1370-1381.

Matoza, R.S., et al., 2022. Atmospheric waves and global seismo-acoustic observations of the January 2022 Hunga eruption, Tonga. *Science*, doi:10.1126/science.abo7063.

Marchand, R.T.; Ackerman, T.P.; Moroney, C. (2007). An assessment of Multiangle Imaging Spectroradiometer (MISR) stereo-derived cloud top heights and cloud top winds using ground-based radar, lidar, and microwave radiometers. J. Geophys. Res. 112, D06204. doi: 10.1029/2006JD007091.

Millán, L., Santee, M. L., Lambert, A., Livesey, N. J., Werner, F., Schwartz, M. J., et al. (2022). The Hunga Tonga-Hunga Ha'apai Hydration of the Stratosphere. *Geophys. Res. Lett. 49,* doi:10.1029/2022GL099381.

Naud, C.M.; Muller, J.-P.; Clothiaux, E.E.; Baum, B.A.; Menzel, W.P. (2005). Intercomparison of multiple years of MODIS, MISR and radar cloud-top heights. *Ann. Geophys. 2005, 23, 2415–2424*. doi: 1432-0576/ag/2005-23-2415.

Nelson, D.L., Garay, M.J., Kahn, R.A., & Dunst, B.A. (2013). Stereoscopic Height and Wind Retrievals for Aerosol Plumes with the MISR INteractive eXplorer (MINX). *Remote Sens. 5, 4593-4628*, doi:10.3390/rs5094593.

Proud, S.R., Parta, A.T., & Schmauß, S. (2022). The January 2022 eruption of Hunga Tonga-Hunga Ha'apai volcano reached the mesosphere. *Science 378, 554–557,* doi:10.1126/science.abo4076.

Rolph, G., A. Stein, and B. Stunder (2017). Real-time Environmental Applications and Display sYstem: READY. *Environmental Modeling & Software 95, 210-228*, doi:10.1016/j.envsoft.2017.06.025.

Sahay, S., J.K. Pati, A.K. Singh, A. Niyogi, M. Chakarvorty, K. Prakash, and M.M. Dwivedi (2023). Characterization of Ash Samples from the Kelud (Indonesia) Volcanic Eruption of 2014 and its Environmental Implications. *Jour. Geol. Soc. India (2023) 99:487-494*. doi: 10.1007/s12594-023-2336-7.

Sellitto, P., Podglajen, A., Belhadji, R., Boichu, M., Carboni, E., Cuesta, J., Duchamp, C., Kloss, C., Siddans, R., Begue, N. & Legras, B. (2022). The unexpected radiative impact of the Hunga Tonga eruption of 15th January 2022. *Nature Comm. Earth & Environ*., doi:10.1038/s43247-022-00618-z.

Smart, D. (2022). The first hour of the paroxysmal phase of the 2022 Hunga Tonga–Hunga Ha'apai volcanic eruption as seen by a geostationary meteorological satellite. *Weather, 77(3), 81-82*, doi:10.1002/wea.4173.

Taha, G., Loughman, R., Colarco, P.R., Zhu, T., Thomason, L.W., and G. Jaross, G. (2022). Tracking the 2022 Hunga Tonga-Hunga Ha'apai aerosol cloud in the upper and middle stratosphere using space-based observations. *Geophys. Res. Lett., 49, e2022GL100091*, doi: 10.1029/2022GL100091.

Themens, D. R., Watson, C., Žagar, N., Vasylkevych, S., Elvidge, S., McCaffrey, A., et al. (2022). Global propagation of ionospheric disturbances associated with the 2022 Tonga volcanic eruption. *Geophys. Res. Lett. 49, e2022GL098158*., doi:10.1029/2022GL098158.

Thompson, A. (2022). Ash blanketing Tonga after volcano eruption creates health concerns. *Scientific American*, 20 January 2022.

Van Eaton, A. R., M. Herzog, C. J. N. Wilson, and J. McGregor (2012). Ascent dynamics of large phreatomagmatic eruption clouds: The role of microphysics, *J. Geophys. Res. 117, B03203*, doi:10.1029/2011JB008892.

Winker, D.M., Pelon, J., Coakley Jr, J.A., Ackerman, S.A., Charlson, R.J., Colarco, P.R., Flamant, P., Fu, Q., Hoff, R.M., Kittaka, C., Kubar, T.L., Le Treut, H., McCormick, M.P., Mégie, G., Poole, L., Powell, K., Trepte, C.,Vaughan, M.A., & Wielicki, B.A. (2010). The CALIPSO mission: A global 3D view of aerosols and clouds. *Bull. Amer. Meteor. Soc., 91, 1211–1229*, doi:10.1175/2010BAMS3009.1.

Witze, A. (2022). Why the Tongan volcanic eruption was so shocking. *Nature 602, 376-378,* doi: 10.1038/d41586-022-00394-y.

Wright. C.J., Hindley, N.P., Alexander, M. J., et al. (2022). Surface-to-space atmospheric waves from Hunga Tonga–Hunga Ha'apai eruption. *Nature*, doi:10.1038/s41586-022-05012-5.

Zhu, Y., Bardeen, C., Tilmes, S., Mills, M., Jarvey, V., Taha, G., Kinnison, D., Yu, P., Rosenlof, K., Wang, X., Avery, M., Kloss, C., Li, C., Glanville, A., Millan, L., Drshler, T., Portmann. R., Krotkov, N., & Toon, O.B. (2022). Perturbations in stratospheric aerosol evolution due to the water-rich plume of the 2022 Hunga-Tonga eruption. *Nature Comm. Earth & Environ*., doi:10.1038/s43247-022-00580-w.

Zuo, M., Zhou, T., Man, W., Chen, X., Liu, J., Liu, F., & Gao, C. (2022). Volcanoes and Climate: Sizing up the Impact of the Recent Hunga Tonga-Hunga Ha'apai Volcanic Eruption from a Historical Perspective. *Adv. Atmos. Sci.,* doi:10.1007/s00376-022-2034-1.

Figure Captions

Figure 1. MISR Hunga Tonga—Hunga Ha'apai Volcano-plume-observation *Locations*, *Dates*, and Terra satellite *Orbit numbers*; the volcano is indicated with a red star. Observations of the mid-stratosphere layer, at ~23-30+ km, are shown in blue markers, those of the near-tropopause layer, at ~11-18 km, are shown in green. The red dot shows where non-spherical particles were retrieved at 10-14 km within a day of the main eruption, most likely dominated by volcanic ash, and the gray dot shows where light-absorbing particles were retrieved, probably smoke originating from wildfires in Australia that might have mixed with the volcanic plume. All other retrievals reported spherical, non-light-absorbing particles, typical of volcanic sulfate/water particles. The open circle marks a downwind plume for which MISR plume heights were retrieved, but the AOD was too low for particle property retrievals.

Figure 2. MISR MINX Plume-height and Wind Vector retrieval results for 15 January 2022 at ~22:05 UTC, Terra Orbit 117440. (a) MODIS context image, with MISR 45˚ forward view superposed (between the orange lines). The volcano location is indicated by a red star. (b) MISR MINX plume-height map, superposed on MISR nadir-view image. (c) MISR-retrieved plume-height profile, starting point on the east side of the MISR field-of-view. (d) Cross-track (roughly west-east) and (e) along-track (roughly south-north) MISR-retrieved wind vector components, assessed over all plume points in the digitized region. (Although this plume segment was observed by MISR to the west of the volcano, the retrieved positive zonal wind indicates eastward motion. The zonal winds varied in elevation and time on this day, and an eastward component at the location and time of the MISR observation is supported by National Center for Physical Acoustics reanalysis (NCPA, https://g2s.ncpa.olemiss.edu/). For all other cases in this study, the MISR-retrieved zonal wind is toward the west.) In Panel (c), Red = zero-wind height; Blue = wind-corrected height; Green = surface elevation. No wind-corrected heights were derived for the two lower layers at ~6 km and ~11 km elevation in Panel c, as the origin of digitization was selected for the more prominent layer at ~ 12 km.

Figure 3. MISR Research Algorithm particle property retrieval results for 15 January 2022, Terra Orbit 117440. (a) MISR context image with study region outlined; the relationship of this region to the HTHH volcano is shown in Figure 2a. (b) AOD at 558 nm in the less cloudy parts of the study region; (c) ANG assessed between 446 and 866 nm; (d) SSA at 558 nm; (e) Non-spherical AOD_{558} fraction. No cost-function filter was applied in this one case, but to improve confidence in the particle property retrieval results, ANG and SSA were assessed over the AOD range $0.15 < AOD_{558} < 8.0$. Digital data for the MISR RA results are given in Table S1.

Figure 4. MISR MINX Plume-height retrieval results for 17 January 2022, Terra Orbit 117456, ~00:25 UTC, acquired north of Queensland, Australia, along with Lucinda AERONET ground-station retrievals. (a) MODIS context image, with MISR 60˚ forward view superposed (between the orange lines). The MISR retrieval region is indicated by the yellow arrow. The location of the Lucinda AERONET station on the northeast Australia coast, marked with a yellow asterisk within the MISR swath, ~450 km south of the over-ocean region where the MISR retrievals were performed, was still apparently within the plume. (For scale, the MISR swath is roughly 380 km wide.) (b) Red-band MISR-MINX plume-height histogram, showing a weak layer near the tropopause at 12-14 km and another near-surface. (c) Blue-band MISR plume-height histogram,

showing a layer at 27-30+ km. (d) CALIOP Level 1, version 4.51, total attenuated backscatter (km^{-1} sr^{-1}) at 532 nm, acquired at ~05:28 UTC on 17 January, roughly 5 hours after and 800 km downwind of the MISR observation at the nearest point. (The inset gives the orbit location, and the red arrow highlights the likely plume layer.) (e) Lucinda AERONET AOD for 24 January 2022, showing the AOD peak on 17 January. (f) Lucinda AERONET AOD for 17 January 2022. (g) Lucinda AERONET Ångström Exponent for 17 January 2022. (AERONET data were provided by Thomas Schroeder and the AERONET team.)

Figure 5. MISR RA particle property retrieval results, same as Figure 3, but for 17 January 2022, Terra Orbit 117456. Note that the scale for panel (e) is logarithmic here to show differences, given the range of in values.

Figure 6. MISR-retrieved Ångström exponent (ANG, inversely proportional to effective particle size) for the MISR observations of the near-source HTHH plume on 15 January (red dot), and for the near-tropopause (green dots) and stratosphere (blue dots and gray dot) plumes downwind. Observation dates and plume heights are given in the annotations.